Journal of Hydro-environment Research 57 (2024) 12–26

Contents lists available at ScienceDirect

Journal of Hydro-environment Research

journal homepage: www.elsevier.com/locate/jher

Research Paper

Real-time prediction of the week-ahead flood index using hybrid deep learning algorithms with synoptic climate mode indices

A.A. Masrur Ahmed [a,b,*], Shahida Akther [c], Thong Nguyen-Huy [d,e], Nawin Raj [b], S. Janifer Jabin Jui [b], S.Z. Farzana [c]

[a] Department of Climate Change, Energy, the Environment & Water, NSW Government, 480 Weeroona Road, Lidcombe NSW 2141, Australia
[b] School of Mathematics, Physics, and Computing, University of Southern Queensland, Springfield, QLD 4300, Australia
[c] Department of Civil Engineering, Leading University, Sylhet 3112, Bangladesh
[d] Centre for Applied Climate Sciences, University of Southern Queensland, Toowoomba, QLD 4350, Australia
[e] Faculty of Information Technology, Thanh Do University, Kim Chung, Hoai Duc, Ha Noi 100000, Vietnam

ARTICLE INFO

Keywords:
Flood index
Climate indices
Deep hybrid learning
Feature extraction
Bangladesh

ABSTRACT

This paper aims to propose a hybrid deep learning (DL) model that combines a convolutional neural network (CNN) with a bi-directional long-short term memory (BiLSTM) for week-ahead prediction of daily flood index (I_F) for Bangladesh. The neighbourhood component analysis (NCA) is assigned for significant feature selection with synoptic-scale climatic indicators. The results successfully reveal that the hybrid CNN-BiLSTM model outperforms the respective benchmark models based on forecasting capability, as supported by a minimal mean absolute error and high-efficiency metrics. With respect to I_F prediction, the hybrid CNN-BiLSTM model shows over 98% of the prediction errors were less than 0.015, resulting in a low relative error and superiority performance against the benchmark models in this study. The adaptability and potential utility of the suggested model may be helpful in subsequent flood monitoring and may also be beneficial to policymakers at the federal and state levels.

1. Introduction

Floods cause considerable damage in South Asia than in any part of the world (Matheswaran et al., 2018). The most affected areas are grasslands, mountain forest ecosystems of the Himalayas, and the Sundarbans (Hasnat et al., 2018). Bangladesh lies geographically at the confluence of three large rivers, the Ganges, Brahmaputra, and Meghna, with about 92.5 % of the basin area outside its boundaries (Khairul et al., 2022). Most of the monsoon rainfall and its water runoff flow through its river network, which might severely exceed the capacity of the drainage channels and cause flooding. Examples of major flood events are 1954, 1955, 1974, 1987, 1988, 1998, 2004, 2007, and 2012, which inundated from 20.5 % up to 70 % of the country on average (Alam et al., 2021). Therefore, it is essential to quantify the direct and indirect costs and hazards of floods to take primitive measures before the events, which requires predictive information of flood characteristics, for example, the start time (flood onset), duration, volume, and peak level.

Because of the high probability and massive impact of flood events, the success of seasonal forecasts and the warning system is critical in seasonal flood management in Bangladesh (Chowdhury, 2005). Accurate and timely prediction of floods can help the relevant stakeholders minimize their drastic effects. Furthermore, government policies can be drawn to identify various options for mitigation. For example, successful flood policies will strengthen relevant planning and implantation agencies (Brammer, 1990). Thus, there is tremendous potential for hydrologic models to be helpful in various applications, particularly in the context of flood preparedness and planning for future climate variability.

Many flood inundation models have been developed recently and effectively implemented in various parts (Bhagabati and Kawasaki, 2017). Despite such models can simulate detailed flood dynamics, they suffer from several significant shortcomings. The significant restrictions of flood inundation models consist of the requirement of complicated

* Corresponding author at: Department of Climate Change, Energy, the Environment & Water, NSW Government, 480 Weeroona Road, Lidcombe NSW 2141, Australia.
E-mail addresses: masrur.ahmed@environment.nsw.gov.au (A.A. Masrur Ahmed), shahidafarheen196@gmail.com (S. Akther), thong.nguyen-huy@unisq.edu.au, nhthong@thanhdoui.edu.vn (T. Nguyen-Huy), nawin.raj@usq.edu.au (N. Raj), sjanifer.jui@usq.edu.au (S. Janifer Jabin Jui), zehan_farzana@lus.ac.bd (S.Z. Farzana).

https://doi.org/10.1016/j.jher.2024.09.001
Received 11 June 2023; Received in revised form 31 March 2024; Accepted 18 September 2024
Available online 25 September 2024

Nomenclature

ABMR	All Bangladesh Monsoon Rainfall
ACF	Autocorrelation Function
ANN	Artificial Neural Network
AO	Arctic Oscillation
AWRI	Available Water Resources Index
BiLSTM	Bi-directional Long Short-Term Memory
BMD	Bangladesh Meteorological Department
BOB	Bay of Bengal
BOM	Australian Bureau of Meteorology
BWDB	Bangladesh Water Development Board
CNN-BiLSTM	Hybrid Model integrating the CNN with BiLSTM
CCF	Cross Correction Function
CNN	Convolutional Neural Network
DL	Deep Learning
DMI	Dipole Model Index
EMI	El Niño Southern Oscillation Modoki Index
ENSO	El Niño Southern Oscillation
EPI	East Pole Index
E_P	Effective Precipitation
FC	Fully Connected
GBI	Greenland Block Index
GRU	Gated Recurrent Unit
I_F	Flood Index
IOD	Indian Ocean Dipole
IPO	Interdecadal Pacific Oscillation
KNMI	Royal Netherlands Meteorological Institute
LM	Legates-McCabe's Index
LSTM	Long Short-Term Memory
MAE	Mean Absolute Error
MAPE	Mean Absolute Percentage Error
MSE	Mean Squared Error
NAO	North Atlantic Oscillation
NCA	Neighbourhood Component Analysis
NOAA	National Oceanic and Atmospheric Administration
NSE	Nash–Sutcliffe Efficiency
NSW	New South Wales
PACF	Partial Autocorrelation Function
PDO	Pacific Decadal Oscillation
QGIS	Quantum GIS
r	Correlation Coefficient
RAM	Random Access Memory
ReLU	Rectified Linear Unit
RMSE	Root-Mean-Square-Error
SAM	Southern Annular Mode
SGD	Stochastic Gradient Descent Optimization
SOI	Southern Oscillation Index
SST	Sea Surface Temperature
STR	Subtropical Ridge
SVR	Support Vector Regression
TPI	Tri-pole Index
WPI	West Pole Index

data inputs, computational effort, and differences in modelling results (Teng et al., 2017).

The flood index (I_F) is an alternative candidate for supporting disaster management and flood risk assessment in simplicity and practical applicability (Cian et al., 2018). The development of I_F often requires simple inputs such as streamflow or precipitation. The I_F has been demonstrated to be a reliable and effective mathematical tool for determining whether or not a given area is flooded at a specific time and location (Quintero et al., 2020). The I_F has also been successfully implemented to monitor flood conditions and characteristics (Moishin et al., 2021b). The reliable and accurate prediction of I_F is critical for early warnings that different societies can use for better management and mitigation.

Prediction of I_F using artificial intelligence methods has developed rapidly in recent years. For example, Prasad et al. (2021a) proposed an M5 tree-based machine learning (ML) model integrated with advanced multivariate empirical mode decomposition to predict daily I_F values in Lockyer Valley in southeast Queensland, Australia. Moishin et al. (2021a) developed a hybrid deep learning (DL) model, combining Convolutional Neural Network (CNN) and Long Short-Term Memory (LSTM) to predict the daily I_F in Fiji. The results indicated that the hybrid DL model outperformed the standalone model (LSTM) and machine learning model (Support Vector Regression). Technically, DL models employ many feature extraction layers to efficiently extract nonlinear and complex compound connections from data (Ghimire et al., 2022). Additionally, DL algorithms are highly effective in extracting data attributes when handling enormous volumes of complicated data and possessing strong computational and sophisticated mapping capabilities (Ghimire et al., 2023c).

Several studies have demonstrated the influence of large-scale climate indices on monsoon precipitation in the Indian subcontinent, however varying depending on the geographic variation of the region (Kumar et al., 1999; Roy and Tedeschi, 2016; Xavier et al., 2007). Han and Webster (2002) showed that the Indian Ocean Dipole (IOD) occurrences significantly influence sea-level changes in the Bay of Bengal and that sea level anomalies in the northern bay may be a predictor of flooding and cholera outbreaks in Bangladesh. Gill et al. (2015) studied correlations between seasonal rainfall and Pacific Sea surface temperatures (SSTs) to reveal spatially distinct relationships between El Niño–Southern Oscillation (ENSO) and Indian summer monsoon rainfall over the entire monsoon season, as well as three sub-seasons. Furthermore, the interactions between large-scale climate indices, e.g., IOD and ENSO can affect the relationship between individual climate indices (e.g., ENSO) and Indian summer monsoon rainfall (Nguyen-Huy, 2020; Pothapakula et al., 2020). Because of the well-known complicated relationship between the monsoon season and ENSO, the large-scale climate drivers likely have a significant role in regulating the food potential of Bangladesh (Ghose et al., 2021; Islam et al., 2021).

This research aims to examine how the extreme phases of climate indices affect the week ahead I_F in the region of Bangladesh. We developed a novel hybrid DL model (i.e., CNN-BiLSTM) by incorporating a Neighbourhood Component Analysis (NCA) algorithm to optimise the significant predictors. The DL methods such as LSTM and gated recurrent networks (GRU) have shown an effective predictive methodology in hydrology and water resources (Ahmed et al., 2021a; Ahmed et al., 2021b). Moreover, the CNN algorithm can extract relevant features of the predictor variables (Ghimire et al., 2023b). In the past research (Ahmed et al., 2021a; Ghimire et al., 2023a), incorporating CNN and an LSTM or GRU model has shown significant performance in predicting hydrological variables. Nonetheless, to our best knowledge, such incorporation has not been piloted in I_F prediction yet, particularly in Bangladesh. Thus, this research addresses the gap in research that needs to be taken for developing countries such as Bangladesh using advanced DL methodology for extreme weather events.

2. Theoretical overview of data intelligent models

2.1. Convolutional neural network (CNN)

The Convolutional Neural Network (CNN) is proposed by LeCun

et al. (1989). CNN reduces parameters and overfitting risk by processing input data via local connections and parameter sharing (Zang et al., 2020). CNN has been extensively used in image recognition, natural language processing, and time series prediction (Ahmed et al., 2021a; Ahmed et al., 2021b; Cannizzaro et al., 2021).

A convolutional layer in CNN incorporates various convolution kernels for extracting different features. Convolutional and pooling layers combine to minimise parameters and accelerate computations (Ghimire et al., 2022). The fully connected layer then uses the convolution kernel's features to calculate the final prediction. Additionally, in the fully connected layer of the architecture, all of the parameters for logic inference are learned from training data (Ghimire et al., 2023b). The mathematical notation of feature extraction by one-dimensional convolution is explained as:

$$a_j^{(l+1)}(\tau) = \sigma(b_j^l + \sum_{f=1}^{F^l} K_{jf}^l(\tau) * a_f^l(\tau)) = \sigma(b_j^l + \sum_{f=1}^{F^l}[\sum_{p=1}^{p^l} K_{jf}^l(p) a_f^l(\tau - p)]) \quad (1)$$

where $a_j^{(l+1)}(\tau)$ denotes feature map j in layer l, σ means non-linear function, F^l denotes number of feature maps in layer l, K_{jf}^l denotes the kernel convolved over feature map f in layer l to create the feature map j in layer $l+1$, p^l denotes the length of kernels in layer l and b_j^l denotes a bias vector. Fig. 1 provides the basic architecture of CNN model.

2.2. Bi-directional long short-term memory (BiLSTM)

Bi-directional long short-term memory (BiLSTM) is a long short-term memory architecture with LSTM layers in forward and backward directions (Peng et al., 2021). BiLSTM uses forward and backward LSTM layers in its architecture, as seen in Fig. 2(b). Each memory block has two LSTM layers. The created two hidden-layer states have opposing temporal sequences using the forward LSTM layer $S_t, t \in [1, T]$ and the backward LSTM layer $S_t', t \in [T, 1]$. These layer states are then combined to deliver the identical output (Ahmed et al., 2022). The forward and backward LSTM layers, respectively, can learn about the past and future of the input sequence (Wang et al., 2019).

The hidden layer state H_t of BiLSTM at time t contains forward $\overrightarrow{h_t}$ and backward $\overleftarrow{h_t}$:

$$\overrightarrow{h_t} = \overrightarrow{LSTM}(h_{t-1}, x_t, c_{t-1}), t \in [1, T] \quad (2)$$

$$\overleftarrow{h_t} = \overleftarrow{LSTM}(h_{t+1}, x_t, c_{t+1}), t \in [T, 1] \quad (3)$$

$$H_t = [\overrightarrow{h_t}, \overleftarrow{h_t}] \quad (4)$$

Here, T is the time series. The BiLSTM method has been successfully applied in hydrological prediction (Kang et al., 2020; Li et al., 2021; Prasad et al., 2018).

2.3. Support vector regression (SVR)

When dealing with limited sets of variables and pattern recognition with a high degree of dimension, Support Vector Regression (SVR) can solve problems. This technique depends on using a kernel function in a high-dimensional space (Ghimire et al., 2022; Prasad et al., 2021b). To calibrate the error between the kernel function and the target data, the relaxation and penalty coefficients are introduced. (Hamidi et al., 2015). For a particular training X, the input is first mapped onto a high-dimensional feature space ϕ(x) (kernel function). After that, it follows a similar structure of a linear model. The linear vector expression can be as follows:

$$f(x) = \omega \bullet \varnothing(x) + b \quad (5)$$

where the weight vector, the constant, and the mapping function of non-linear transformation are ω, b, and ϕ(x), respectively. By reducing the model complexity, the constant b and coefficient ω are estimated by diminishing:

$$R_{reg}(f) = C\frac{1}{N}\sum_{i=1}^{N} L_\varepsilon(f(x_i), y_i) + \frac{1}{2}\|w\|^2 \quad (6)$$

$$L_\varepsilon(f(x) - y) = \begin{cases} |f(x) - y| - \varepsilon for |f(x) - y| \geq \varepsilon \\ 0 otherwise \end{cases} \quad (7)$$

Here, both the parameters C and ε are to be determined which influence the generalization performance, and the loss function assesses estimation quality $L_\varepsilon(f(x_i), y_i)$, known as ε intensive loss function. $C\frac{1}{N}\sum_{i=1}^{N} L_\varepsilon(f(x_i), y_i)$ is the empirical error and $\frac{1}{2}\|w\|^2$ is the smoothness of the function. The trade-off between the experimental threat and the smoothness of the model is denoted by C. Moreover, the dual problem, given as transfer the optimization problem:

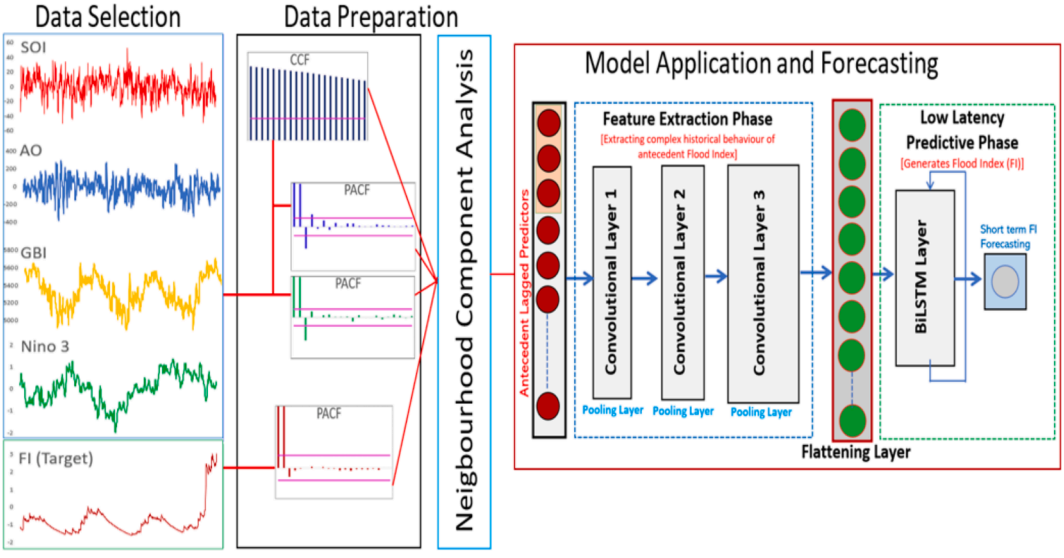

Fig. 1. Schematic workflows of the CNN-BiLSTM hybrid model integrating neighborhood component analysis (NCA). The hybrid CNN-BiLSTM integrates convolution neural network (CNN) and bi-directional long short-term memories (BiLSTM).

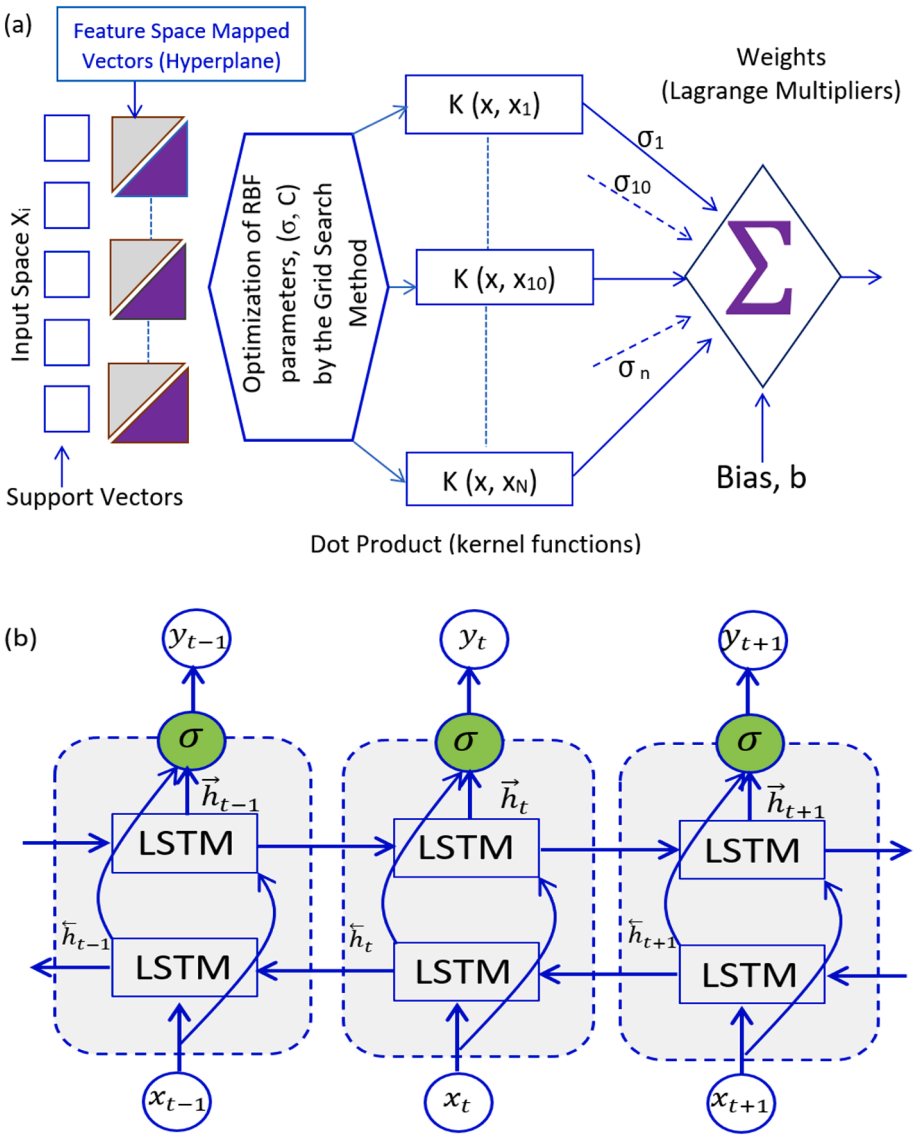

Fig. 2. (a) Schematic structure of support vector regressions (SVR) and (b) Schematic structure of bidirectional LSTM (BiLSTM).

$$f(x) = \sum_{i=1}^{l} (\alpha_i - \alpha_i^*) k(x_i, x) + b \tag{8}$$

where, α_i and α_i^* are the introduced Lagrange multipliers and $k(x_i, x)$ is the kernel function. The schematic structure of SVR is illustrated in Fig. 2(a).

2.4. Neighbourhood component analysis (NCA)

Feature selection plays a crucial role in developing predictive models. This is because it enables a reduction in the number of input variables, thereby minimizing processing costs, and improving the accuracy and interpretability of the model in terms of its properties and predictors (Bowden et al., 2005; Maier et al., 2010; Prasad et al., 2018; Yang et al., 2012). This study used Neighbourhood Component Analysis (NCA) to separate significant antecedent lagged predictor variables from potential input variables. This method was developed by Yang et al. (2012) and is non-rectilinear and non-parametric.

The NCA feature selection was performed using the *fsrnca* algorithm in MATLAB with regularization, which was aimed at learning feature weights that minimize the average leave-one-out regression loss across the training data. Through the NCA process, we trained a variable set to obtain a better understanding of the characteristics by weighting and minimizing the objective function while computing regression loss for soil moisture prediction.

In the *fsrnca* algorithm, a function $g(x) : \boldsymbol{R^P} \rightarrow \boldsymbol{R}$ is utilized to predict the response y based on several input variables, optimizing their nearest spaces. The weighted distance (D_w) between any two samples in the training set $T = \{(x_i, y_i) : i = 1, 2, 3, \cdots, N\}$, where $x_i \in \boldsymbol{R^P}$ is the feature vectors (i.e., predictor variables) and $y_i \in \boldsymbol{R}$ is the target (i.e., the response variable), is calculated as follows:

$$D_w(x_a, x_b) = \sum_{j=1}^{J} w_j^2 |x_a, x_b| \tag{9}$$

During training, the *fsrnca* algorithm calculates the weighted distance (D_w) between two samples, x_a and x_b, by considering the weight, wj, associated with the jth feature. To improve the accuracy of the leave-one-out prediction during training, a probability distribution, $p_{\alpha\beta}$, is used. This probability represents the likelihood that x_α selects x_β as its reference argument. To select the feature subset and avoid overfitting, the algorithm uses a weighting vector, 'w', in conjunction with the gradient ascent method. A regularization component is included in this process to ensure that the model does not overfit the data. The schematic

structure of BiLSTM is illustrated in Fig. 2(b).

3. Case study description and data

3.1. Study locations

In our study, we validated 34 stations in Bangladesh (Fig. 3(a)) to predict the I_F using a hybrid DL model (i.e., CNN-BiLSTM). Bangladesh is a riverine country situated in the Ganges Delta, having a sub-tropical monsoon climate. Bangladesh lies in a unique position (20°45′N to 26°40′N and from 88°05′E to 90°45′E) where northern Bangladesh is in the foothills of the Himalayas, located in the Meghalaya Plateau, the Assam hill in the East, the Gangetic plain in the West and the Bay of Bengal in the South (Ahmed and Kim, 2003). The average annual rainfall varies between 2100 to 5100 mm, and 80 % occurs during the monsoon (June to October) (BWDB, 2019). Bangladesh has 80 % of the land in the floodplain areas, and over 50 % is within 5 m above sea level (Chowdhury, 1998; Rahman, 2010). Due to heavy rainfall and eventual flooding, the country suffers enormous impacts on its agriculture, economy, infrastructure, and population (Tingsanchali and Karim, 2005).

3.2. Flood Index (I_F)

The daily rainfall (mm) of 34 weather stations in Bangladesh was acquired from the Bangladesh Meteorological Department's Climate Division. In this study, the flood index (I_F), as the response variable of our proposed DL model, is estimated from the effective precipitation (E_P) followed by the principle in a recently published relevant study (Lu, 2009; Nguyen-Huy et al., 2022). Suppose E_m was the rainfall reported on any day, where m is between 1 and 365 and the summation length of the preceding day is N, E_P for that (current i^{th}) day over a duration D was:

$$E_{P_i} = \sum_{N=1}^{D} \left[\frac{\sum_{m=1}^{N} E_m}{N} \right] \tag{10}$$

In order to calculate the total amount of recent and accumulated precipitation, daily water loss (due to runoff, evapotranspiration, infiltration, etc.), and the length of accumulation, the Available Water Resources Index ($AWRI$) (Byun and Lee, 2002) is expressed as a function of weighting factor W summed over that duration:

$$AWRI = \frac{E_p}{W} \tag{11}$$

$$W = \sum_{N=1}^{N=D} \frac{1}{N} \tag{12}$$

In this study, we used the duration of 365 (D) days (ignoring the leap year for simplicity) as for the usual hydrological cycle and hence Equation (11) can be written as:

$$AWRI = E_1 + \frac{(W-1)E_2}{W} + \frac{(W-1-\frac{1}{2})E_3}{W} + \cdots + \frac{W-1-\frac{1}{2}-\cdots-\frac{1}{364})E_{365}}{W} \tag{13}$$

$$\approx E_1 + 0.85E_2 + 0.77E_3 + \cdots + 4.23{*}10^{-4}E_{365}$$

In order to account for the gradual depletion of available water supplies, equation (13) incorporates the E_P into an exponential time-dependent reduction function. The current day incorporates 100 % of the precipitation received from the preceding day. Furthermore, it takes into account around 85 % of the rainfall that happened two days prior, and roughly 77 % of the precipitation from three days ago, and this endures in a decreasing fashion until it includes approximately 0.042 % of the precipitation that happened 365 days before. This is consistent with the

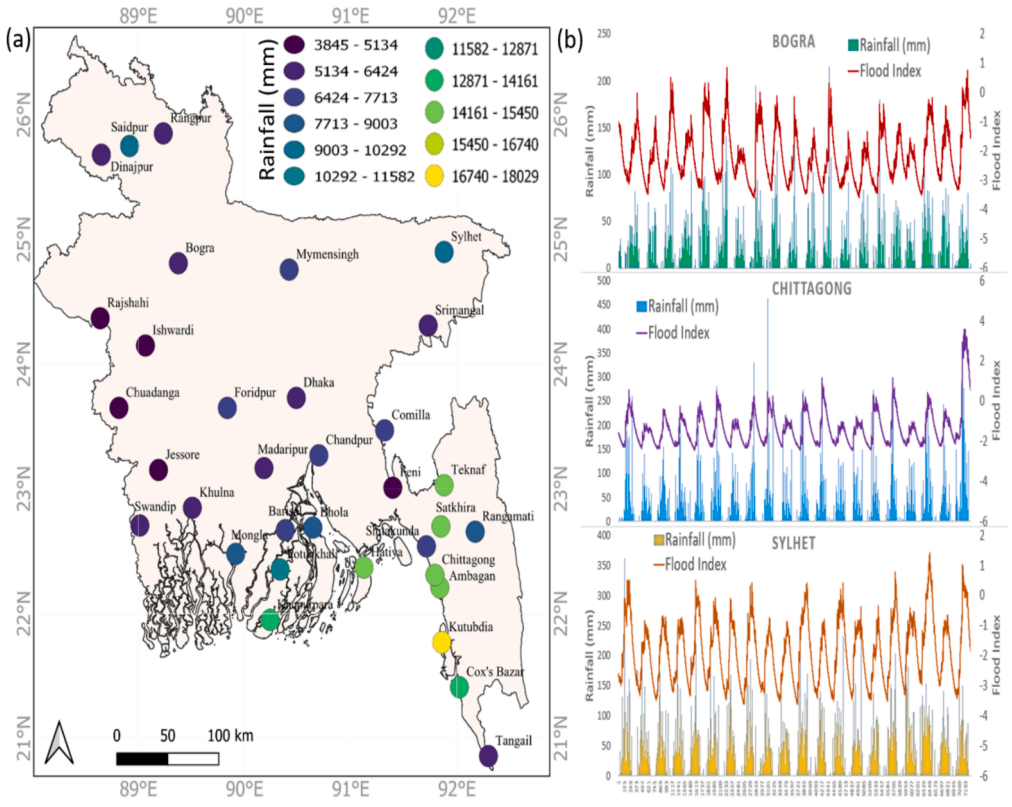

Fig. 3. (a) The selected weather stations of Bangladesh with total rainfall of 2019, (b) Time series plot of rainfall (mm) vs. the flood index (I_F) of three selected stations (i.e., Bogra, Chittagong, and Sylhet). Note: the list of geographical locations of the stations is tabulated in Table 1.

physical rationale for diminishing water supply, as in rainfall-runoff models and the latest studies of flood detection using daily data (Lu, 2009). However, this Equation is much simpler than rainfall-runoff models as it is useful for detecting whether there is an excess or shortage of water supplies that could lead to a flood catastrophe. This empirical model employs simply precipitation data and does not need any parameter estimates, unlike rainfall-runoff models, which have more complex data input specifications (Deo et al., 2018).

Reduced weight means the depletion of water supplies due to hydrological cycles. A few days after a rainstorm event, the loss of water resources is anticipated to reach its peak (Moishin et al., 2021b). This perspective assumes that recent downpours have a substantial impact on the risk of a flood. However, the proposed approach considers the accumulated impacts of previous rainfall fairly. Generally, if the AWRI exceeds the average, the water supplies are relatively ample, indicating the risk of flooding (Han and Byun, 2006). As such, the Flood Index (I_F), a standardized metric, is expressed by equation (14):

$$I_F = \frac{ARWI - {}^{1983}_{2020}\overline{ARWI^{max}}}{\sigma({}^{1983}_{2020}\overline{ARWI^{max}})} \tag{14}$$

where ${}^{1983}_{2020}\overline{ARWI^{max}}$ is the mean of annual maximum daily *AWRI* for the determined period 1983–2020 and $\sigma({}^{1983}_{2020}\overline{ARWI^{max}})$ is the standard deviation. In light of this, the criterion of the daily I_F being more than zero can be used to determine the risk of flooding on any given day.

The severity of a flood event can be evaluated based on the sum of positive I_F values from the onset of the flood [t_{onset} i.e., the first day when $I_F > 0$] to its end [t_{end}, last day before$I_F < 0$]. The highest event of flood danger I_F^{max} is determined by identifying the maximum value of I_F from t_{onset} and t_{end}. The duration of the flood event, D_F, can be measured by calculating the number of days between t_{onset} and t_{end}. Notably, various characteristics of flood events can be measured and evaluated using a straightforward running-sum approach (Yevjevich, 1967):

$$I_F^{acc} = \sum_{t=t_{onset}}^{t=t_{end}} I_{F_t} \text{ t where } I_{F_t} > 1 \tag{15}$$

$$I_F^{max} = \max(I_F)_{t_{end}-t_{onset}} \tag{16}$$

$$D_F = t_{end} - t_{onset} \text{ (days)} \tag{17}$$

During a period of flooding, the index of the flood for a particular day t is denoted by I_{F_t}, and it is only relevant when$I_F > 0$ and $t_{onset} \leq t \leq t_{end}$. The regular I_F observed during the study period is a time-varying signal that generates positive or negative index values in response to significant (or low) rainfall, as established by Nosrati et al. (2010). A positive value of I_F indicates a flooding event, and the flood properties are analyzed during this period of flooding.

3.3. Large-scale climate indices

Fifteen large-scale daily climate indices were utilised as predictor variables to anticipate the I_F using a hybrid DL CNN-BilSTM model. Table 1 provides the list of climate indices and respective sources. Fig. 4 shows a map of the research area with oceanic representation used to determine the climatic mode indices.

3.4. Development of hybrid CNN-BiLSTM model

The CNN-BiLSTM integration synergises the strengths of each model element. CNN is used to handle spatial patterns (i.e., low-level features) in the data while BiLSTM is used to capture temporal patterns and dependencies over time (i.e., sequential relationships). Specifically, in the CNN model, patterns like edges, textures, or shapes in local regions of the input are detected through convolutional layers. The dimensions of spatial information are then reduced in pooling layers, preserving the most important features, which are finally converted into a flat vector as the input of the BiLSTM model. In the BiLSTM model, the forward LSTM processes the input sequence from the beginning to the end, capturing past context while the backward LSTM deals with the input sequence in reverse, capturing future context. The final output represents combining spatial and temporal information. The schematic workflows of the CNN-BiLSTM hybrid model are illustrated in Fig. 1. The optimum architectures of the hybrid CNN-BiLSTM and BiLSTM-based predictive model are tabulated in Table 2.

Table 1
Twelve climate model indices were used as predictor variables to forecast the flood index using the hybrid deep learning CNN-BiLSTM predictive model combining a convolutional neural network (CNN) and a bi-directional long-short term memory (BiLSTM). Source of data: monthly sea surface temperature (SST) in different oceanic regions derived from the Optimum Interpolation SST, version 2 (OISST v2) downloaded from Climate Prediction Center (CPC, NOAA).

Variable	Name and Description	Data Source
Niño 3	Average SST over 150°–90 °W and 5 °N–5 °S	OISST v2, NOAA
Niño 3.4	Average SST over 170 °E–120 °W and 5 °N–5 °S	OISST v2, NOAA
Niño 4	Average SST over 160 °E–150 °W and 5 °N–5 °S	OISST v2, NOAA
Niño 1 + 2	Average SST over 90°W–80°W and 0°–10°S	OISST v2, NOAA
AO	Arctic Oscillation	NCEP
DMI	DMI=WPI – EPI WPI=Average SST over 50°–70°E & 10°N–10°S EPI=Average SST over 90°–110°E & 0°N–10°S	OISST v2, NOAA
EMI	EMI=C – 0.5 x (E+W) Where the components are average SSTA over C: 165 °E–140 °W and 10 °N–10 °S E: 110°–70°W and 5 °N-15°S W: 125°-145 °E and 20 °N-10 °S	ERRSST. v.3b
NAO	North Atlantic Oscillation	NCEP
PDO	Pacific Decadal Oscillation	NCEP
SAM	Southern Annular Mode index	NCEP
SOI	Southern Oscillation IndexThe pressure difference between Tahiti and Darwin as defined by Troup (1965)	BOM
TPI	Tripole Index for the Interdecadal Pacific Oscillation	NCEP
RMM1	Real-time Multivariate MJO series 1	
RMM2	Real-time Multivariate MJO series 2	
GBI	Greenland Block Index	NCEP

Note: EMI=ENSO Modoki Index; WPI=West Pole Index; EPI=East Pole Index; DMI=Dipole Model Index,

The proposed CNN-BiLSTM model was developed with a 3.6 GHz Intel i7 processor and 16 GB of RAM machine. The Python interface of the models uses *TensorFlow* (Abadi et al., 2016) and *Keras* (Ketkar, 2017) DL frameworks to generate a multi-phase CNN-BiLSTM model. Keras is a DL API that integrates with TensorFlow, a capable Python machine learning framework. Keras is a highly usable interface for modern DL techniques. Also, NCA is implemented in MATLAB R2020b. The predicted I_F is also visualised using *matplotlib* (Barrett et al., 2005) and *seaborn* (Waskom et al., 2020). Quantum GIS (QGIS) software was also utilised to visualise the study area and geographical plots. A list of nine statistical measures is employed to investigate the practical implications of forecasting models. The following stages were taken in the creation of the proposed CNN-BiLSTM model.

3.4.1. Selection of predictor variables

Correlation between the predictors serve as a crucial tool in climatological research, which is essential for identifying key predictors in complex climate systems. In the Chittagong climate dataset, as shown in Fig. 5, "GBI" shows the most significant positive correlation with the target variable 'I_F', recording a coefficient of approximately 0.44. This suggests 'GBI' as a potential primary predictor of 'I_F'. In contrast, the Nino indices—indicators of the El Niño phenomenon—exhibit only marginal correlations with 'I_F', with 'NINO4' presenting a slight

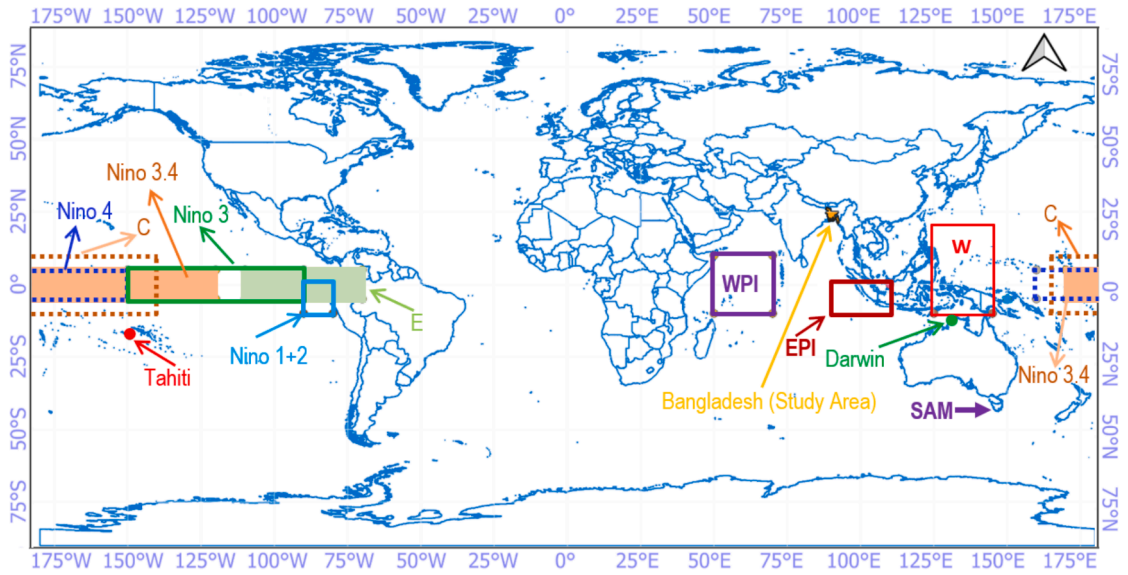

Fig. 4. Map of the study region with oceanic representation used to calculate the climate mode indices (CI). The details of the climate mode indices are provided in Table 2.

Table 2
The optimum architecture of the hybrid CNN-BiLSTM and BiLSTM-based predictive model developed through a trial error procedure. *Note*: ReLU stands for Rectified Linear Units, SGD stands for Stochastic gradient descent optimizer.

Hyper-parameter	Optimal Hyper-Parameters	
	CNN-BiLSTM	**BiLSTM**
Convolution Layer 1 (C1)	70	
C1- Activation function	ReLU	
C1-Pooling Size	1	
Convolution Layer 2 (C2)	60	
C2– Activation function	ReLU	
C2-Pooling Size	1	
BiLSTM Layer 1 (L1)	55	60
L1- Activation function	Tanh	Tanh
BiLSTM Layer 2 (L2)	80	60
L2- Activation function	ReLU	ReLU
Drop-out rate	0.2	0.2
Optimiser	SGD	SGD
Padding	Same	Same
Batch Size	5	7
Epochs	1000	1000

negative correlation and 'NINO34' a weak positive one. These findings suggest that while El Niño-related variables have some influence, they do not act as strong individual predictors for 'I_F' in this region. The rest of the dataset variables predominantly display weak or negligible correlations, implying a complex network of relationships that potentially involve non-linear interactions.

Despite the lack of a precise technique to determine whether model predictors are reliable (Tiwari and Adamowski, 2013), to select the time series of I_F's lag-time memories and predictors for an appropriate framework, different techniques are applied. These methods include trial and error, autocorrelation function (ACF), partial autocorrelation function (PACF), and cross-correlation function (CCF) (Masrur Ahmed et al., 2021). A significant antecedent behaviour in terms of the lag of I_F from the predictors was found using the PACF (Tiwari and Adamowski, 2013; Tiwari and Chatterjee, 2011). By monitoring the statistical resemblance between the predictors and the dependent variable, the CCF oversees choosing the input signal pattern based on the antecedent lag of the predictors. For example, Fig. 6 (a) depicts the r_{cross} between I_F and GBI and Niño1 + 2 at Sylhet and Khulna stations. According to the figure, previous monthly delays have been statistically significant. If we look at the climate indices, the GBI revealed significant r_{cross}, ranging from + 0.60 to + 0.68, respectively. To increase the diversity, the correlation coefficient (r) between predictors (i.e., GBI and Niño1 + 2) and target (I_F) is illustrated in Fig. 6(b) and 6(c). It is found that the earliest legs provided comparatively higher correlations.

The NCA method also tests the significant antecedent lag memories of large-scale climate indices and I_F. This method delivers the required improvements in prediction accuracy and understanding of its predictors' predictive model traits and nature while reducing the dimensionality of input variables and computing cost.

3.4.2. *Hybrid CNN-BiLSTM model design*

The proposed hybrid CNN-BiLSTM model is established by using a CNN as spatial feature extraction and a BiLSTM as a temporal predictive model. The primary task is the configuration of hyper-parameters and the optimisation of these parameters. A large number of hyper-parameters must be addressed to develop a successful DL method. For this experiment, the default *Keras* parameters are used for network initialisation. This is the set of default-training parameters: the number of epochs in the training set is 200; the batch size is five, and the look-up size is one. ReLU is applied to the CNN-BiLSTM and BiLSTM networks as an activation function (see Table 2).

In addition, the SGD optimiser is employed, with a learning rate of 0.001. The number of hidden layer units varies between 70 and 60 for all layers of DL models, depending on their architecture. A feature extraction method involving three convolution layers was used, with each layer having its own set of filter and kernel size parameters, such as (70, 4) and (60, 4), respectively. Mean Square Error (MSE) was used as a loss function in the model to represent the error. Aside from that, we scale the predictor variables between 0 and 1 using a min–max normalisation function. The missing values are filled in with the mean value of the same date.

The input data are divided into three sets to develop predictive models: training, testing, and validation. The model is trained on the same data set in each iteration. As a result, the model will better understand the data's features as it is trained. Validation sets are used to analyse and validate models during development as compared to training sets. The information obtained from this validation procedure is meant to be used to change the model hyperparameters as necessary. Finally, the testing phase is used only after a model has been trained (using the train and validation sets), and it is primarily used to evaluate

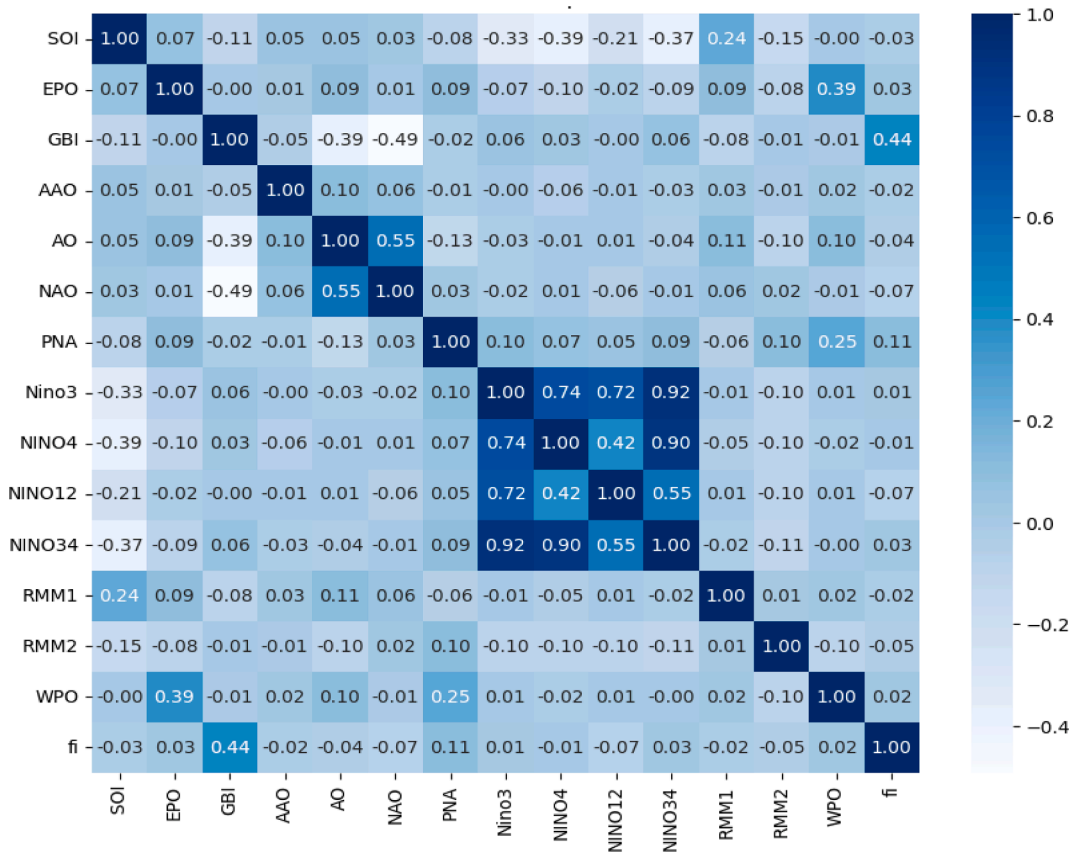

Fig. 5. Correlation Landscape of Climatic Indicators Influencing 'I$_F$' in the Chittagong Region.

the model. 39 years of data were used in this study, and 70 % of the data sets were used for training, 15 % for validation, and 15 % for testing.

3.4.3. Performance metrics

The prediction performance was done by a rigorous and insightful evaluation of the objective model CNN-BiLSTM with other counterpart models. Our study evaluated multiple graphical and statistical metrics in the independent testing phase. The paper uses statistical metrics such as Pearson's correlation coefficient (*r*), Mean Absolute Percentage Deviation (*MAPD*; %), Mean Absolute Error (*MAE*), Root Mean Squared Error (RMSE), and Nash–Sutcliffe Efficiency (*NSE*). The mathematical notations of the statistical parameters are listed below, Eq. (14–17).

$$\text{Mean Absolute Error } (MAE) = \frac{1}{n}\sum_{i=1}^{n}\left|I_F^{for} - I_F^{obs}\right| \tag{8}$$

$$\text{Nash} - \text{Sutcliffe Efficiency } (NSE) = 1 - \left[1 - \frac{\sum_{i=1}^{n}\left(I_F^{for}\right)^2}{\sum_{i=1}^{n}\left(I_F^{obs} - \overline{I_F^{for}}\right)^2}\right] \tag{9}$$

$$\text{Correlation Coefficient}(r) = \left(\sum_{i=1}^{n}\left(I_F^{obs} - \frac{\overline{I_F^{obs}}\left(I_F^{for} - \overline{I_F^{for}}\right)}{\sqrt{\sum_{i=1}^{n}\left(I_F^{obs} - \overline{I_F^{obs}}\right)^2\sum_{i=1}^{N}\left(I_F^{for} - \overline{I_F^{for}}\right)^2}}\right)\right)^2 \tag{10}$$

$$\text{Mean Absolute Percentage Error } (MAPD;\%) = \frac{1}{n}\left(\sum_{n}^{i=1}\left|\frac{\left(I_F^{for} - I_F^{obs}\right)}{I_F^{obs}}\right|\right)*100 \tag{11}$$

$$\text{Root Mean Square Error}(RMSE) = \sqrt{\frac{1}{n}\sum_{i=1}^{n}\left(I_F^{for} - I_F^{obs}\right)^2} \tag{12}$$

$$\text{Percent Bias } (\text{PBIAS},\ \%) = \frac{\sum_{i=1}^{n}\left|I_F^{for} - I_F^{obs}\right|}{\sum_{i=1}^{n}\left(I_F^{obs}\right)} \tag{13}$$

Where I_F^{obs} is the observed and I_F^{for} is the model-predicted value from the i^{th} element; $\overline{I_F^{obs}}$ and $\overline{I_F^{for}}$ show their average, respectively, and n denotes the number of observations of the I_F.

4. Results and discussions

4.1. Results of flood index prediction

We present a deep hybrid predictive model (CNN-BiLSTM) to predict

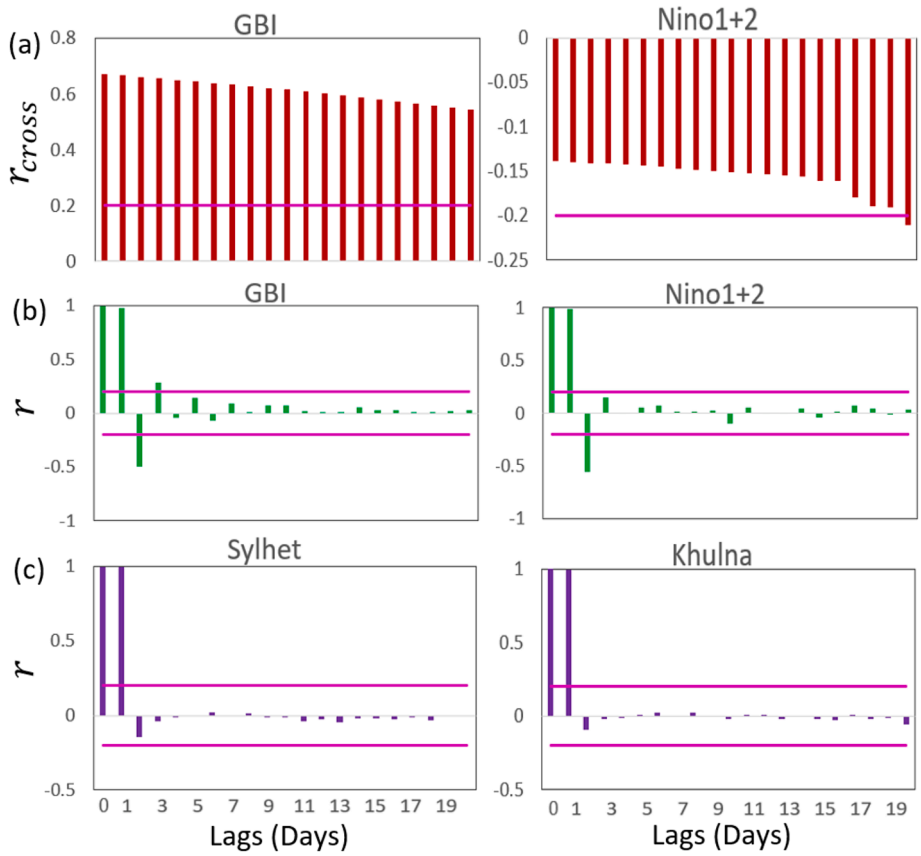

Fig. 6. (a) Cross-correlation functions (CCF) showing the covariance between the objective variable (I_F) and the predictor variables (i.e., GBI and Nino1 + 2) for Sylhet stations, (b) Partial autocorrelation function (PACF) plot of the predictor variables (i.e., GBI and Nino 1 + 2) of Sylhet stations and (c) Partial autocorrelation function (PACF) plot of the target variable (i.e., I_F) of Sylhet and Khulna stations. The pink line in the figures indicates the ± 95 % confidence level.

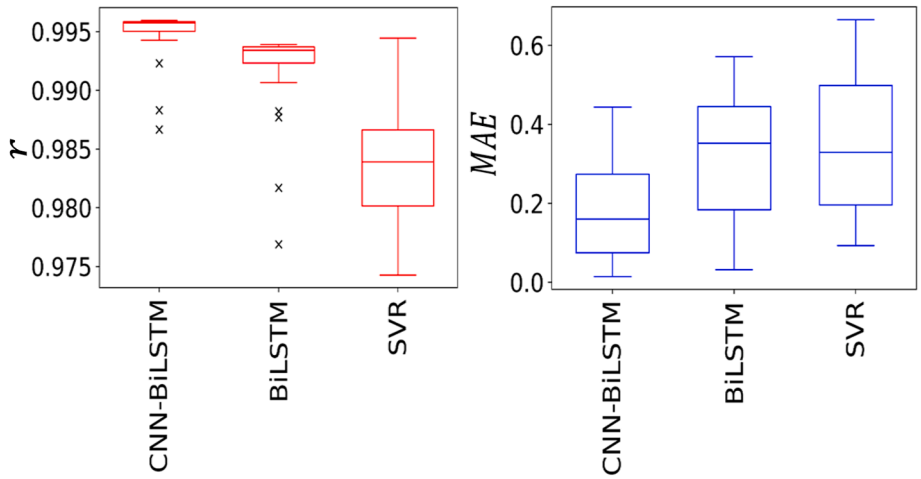

Fig. 7. Box plots of proposed hybrid models (i.e., CNN-BiLSTM) compared with their respective standalone counterparts (i.e., BiLSTM and SVR) in predicting I_F in terms of Correlation Coefficient (*r*) and Mean Absolute Error (MAE) for 34 selected stations in Bangladesh.

the I_F of thirty-four selected stations in Bangladesh, compared with two benchmark models (i.e., BiLSTM and SVR). Statistical metrics and infographics were also used to understand the predictive capability of the proposed model. Overall, the proposed CNN-BiLSTM model was found to predict I_F values using large-scale climate indices accurately.

Fig. 7 shows that, when compared to other benchmark models, the proposed hybrid DL model (CNN-BiLSTM) exhibits significant improvement in I_F prediction for a loop of thirty-four stations, as demonstrated by the evaluation matrices correlation coefficient (*r*) and mean absolute error (*MAE*). The figure also displays better distributions of *r* and *MAE* values of the CNN-BiLSTM model between the lower quartile (25th percentile) and the upper quartile (75th percentile) compared to BiLSTM and SVR, indicating the ability of accurate prediction of the proposed model for all the study sites. In addition, Table 3 shows that the proposed CNN-BiLSTM model yields better *r*-values ≈ 0.987–0.996, which is superior to the BiLSTM model with *r* ≈ 0.977–0.993. On the other hand, the classical machine learning model (i.e., SVR) has lower *r*-values ≈ 0.888–0.992. The same results were

Table 3
The performance evaluation of the proposed hybrid deep learning CNN-BiLSTM vs. benchmarks models (BiLSTM and SVR) at thirty-four stations in Bangladesh by the correlation coefficient (*r*) and mean absolute error (*MAE*) in the testing phase.

Stations	*r*			*MAE*		
	CNN-BiLSTM	BiLSTM	SVR	CNN-BiLSTM	BiLSTM	SVR
Ambagan	0.995	0.991	0.988	0.322	0.423	0.358
Barishal	0.996	0.994	0.983	0.022	0.276	0.293
Bhogra	0.996	0.993	0.982	0.280	0.427	0.571
Bhola	0.996	0.994	0.988	0.045	0.289	0.302
Chandpur	0.995	0.992	0.985	0.195	0.444	0.447
Chottpgram	0.996	0.992	0.978	0.184	0.445	0.485
Chuadanga	0.995	0.992	0.980	0.129	0.180	0.192
Comilla	0.996	0.993	0.974	0.444	0.506	0.665
Cox's Bazar	0.992	0.988	0.987	0.192	0.254	0.237
Dhaka	0.996	0.994	0.987	0.256	0.399	0.503
Dinajpur	0.996	0.994	0.983	0.061	0.116	0.136
Faridpur	0.996	0.992	0.982	0.047	0.083	0.124
Feni	0.996	0.994	0.983	0.406	0.571	0.663
Hatiya	0.988	0.982	0.988	0.153	0.229	0.210
Iswardi	0.996	0.994	0.981	0.161	0.196	0.208
Jessore	0.996	0.993	0.986	0.015	0.065	0.109
Khepurpara	0.994	0.991	0.978	0.362	0.521	0.563
Khulna	0.996	0.993	0.985	0.083	0.135	0.166
Kutbdia	0.995	0.993	0.990	0.115	0.386	0.357
Madaripur	0.996	0.994	0.976	0.165	0.415	0.431
Mongla	0.995	0.988	0.985	0.150	0.419	0.400
Mymenshing	0.996	0.994	0.979	0.226	0.453	0.445
Patuakhali	0.987	0.977	0.988	0.080	0.352	0.279
Rajshahi	0.996	0.993	0.976	0.039	0.047	0.113
Rangamati	0.996	0.994	0.994	0.285	0.548	0.547
Rangpur	0.996	0.994	0.984	0.037	0.033	0.093
Sandwip	0.995	0.993	0.984	0.160	0.201	0.232
Satkhira	0.996	0.994	0.980	0.063	0.118	0.155
Sheetakunda	0.995	0.991	0.986	0.334	0.492	0.561
Srimangal	0.996	0.994	0.985	0.409	0.561	0.659
Sydpur	0.996	0.993	0.979	0.073	0.130	0.150
Sylhet	0.996	0.994	0.989	0.378	0.520	0.628
Tangail	0.996	0.993	0.985	0.111	0.353	0.367

observed using the *MAE*. The proposed hybrid DL prediction model outperforms the other two competing methods as demonstrated by the *r* and *MAE* values.

Fig. 8 contains further information on I_F prediction regarding the coefficient of determination (R^2) and RMSE. In general, the newly developed CNN-BiLSTM model can provide the highest value of R^2 and the lowest values of RMSE. The R^2 values generated by the CNN-BiLSTM model ranged between 0.995 and 0.996 over 80 % of the total stations. The second candidate is the BiLSTM model, with R^2 ranging from 0.977 to 0.992, while the SVR model has the lowest R^2 values of 0.965 to 0.991. Overall stations, the deep hybrid CNN-BiLSTM prediction model outperformed other benchmark models.

Further evaluation of the predictive model (i.e., CNN-BiLSTM) is performed by a scatter plot, as shown in Fig. 9. The scatter plot is plotted with the goodness-of-fit between predicted and observed I_F and a least-square fitting line. As illustrated in Fig. 8, the suggested model outperforms the baseline model by a significant margin, with an R^2 value significantly higher than the baseline model. The proposed hybrid DL model (CNN-BiLSTM) performed noticeably better for the Sylhet station than for the other stations and models in terms of I_F forecasting, recorded the magnitudes that were most like one ($m|R^2 \approx 0.656|0.996$), followed by the BiLSTM (0.627|0.993) model. Additionally, the Comilla station exhibits substantial performance with the proposed CNN-BiLSTM (0.65|0.997) model when compared to the BiLSTM (0.64|0.994), and SVR (0.69|0.974) models, respectively. Hence, it is evident that the DL hybrid CNN-BiLSTM predictive model is well-appropriate for forecasting the week-ahead I_F forecast.

A time series plot does further evaluation; the predictive abilities of the hybrid and standalone models that were used in the study are further established. Fig. 10 compares the predicted and observed I_F time series plot between the proposed hybrid (i.e., CNN-BiLSTM) model and the standalone model (i.e., SVR). To illustrate, Fig. 9 depicts the predicted I_F at two stations using the proposed model and classical machine learning model (i.e., SVR), resulting in an extremely near I_F to the one that was seen, showing that the model is highly predictable. A significant improvement in forecasted I_F was achieved due to the application of the NCA algorithm.

The inclusion of the Taylor diagram (Taylor, 2001) in the study shown in Fig. 11 adds additional support to a more thorough analysis

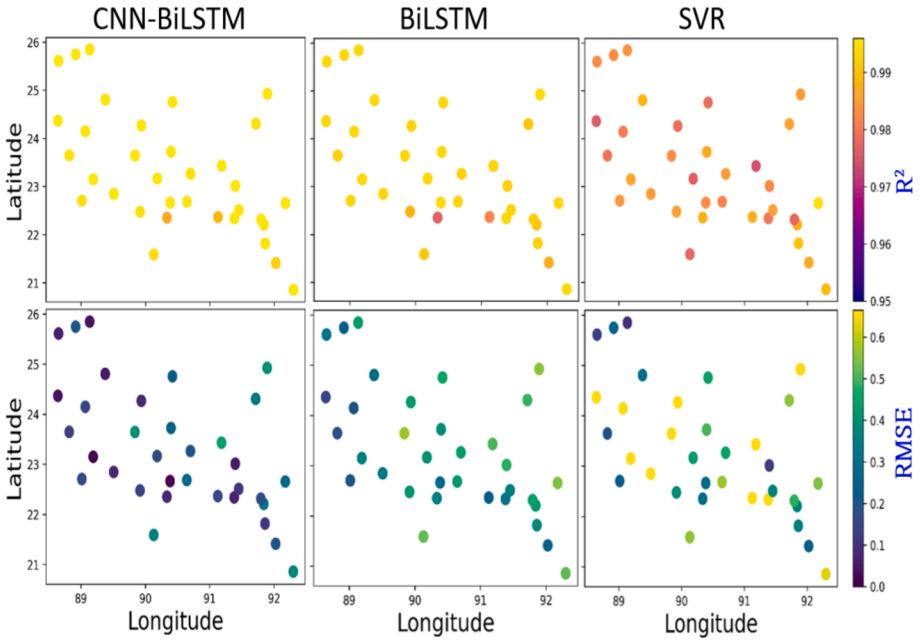

Fig. 8. Geographic distribution of the coefficient of determination (R^2) and root means squared error (RMSE) acquired from the proposed hybrid model (i.e., CNN-BiLSTM) and standalone counterparts (i.e., BiLSTM and SVR) in forecasting I_F across thirty-four stations in Bangladesh.

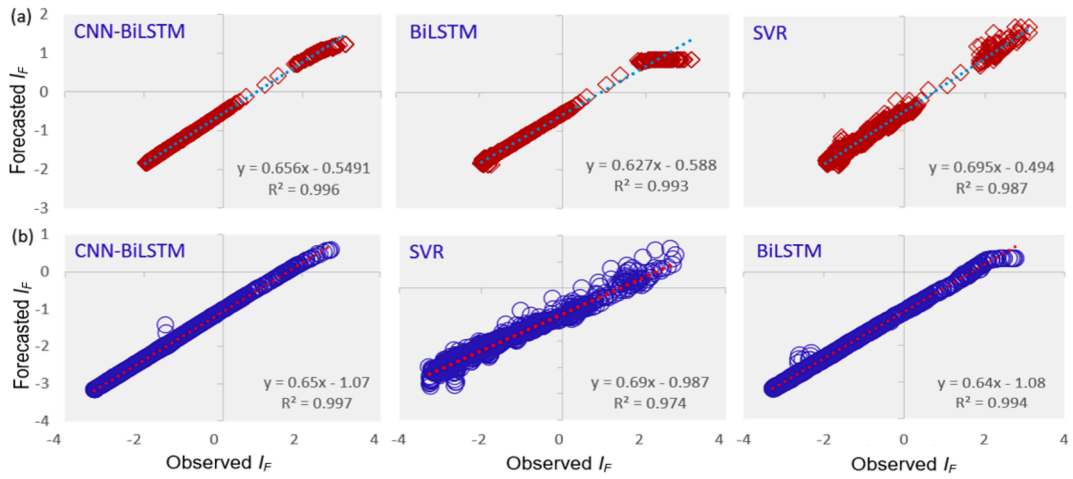

Fig. 9. Scatter plot of forecasted vs. observed I_F of a) Sylhet and b) Comilla sites using the proposed hybrid model (i.e., CNN-BiLSTM) and Standalone models (i.e., BiLSTM and SVR). A least square regression line and coefficient of determination (R^2) with a linear fit equation are shown in each sub-panel.

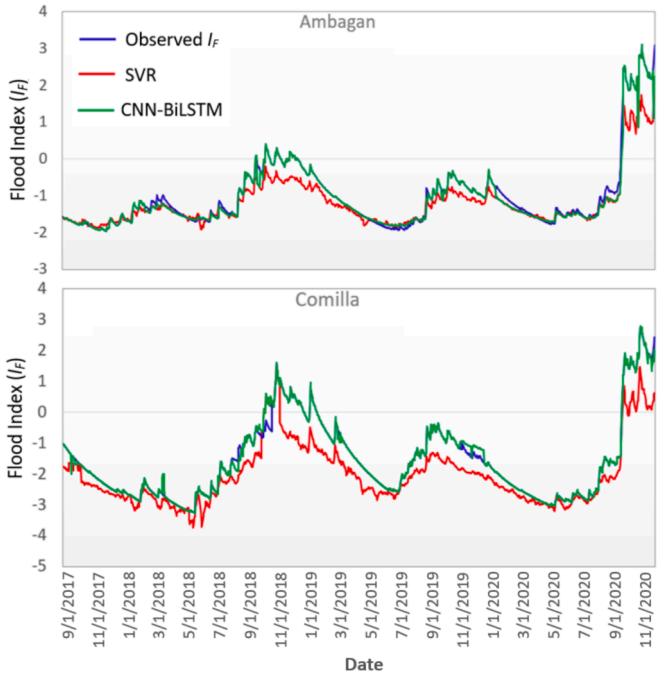

Fig. 10. Comparison of time series distribution between forecasted I_F and observed I_F during model testing phase using CNN-BiLSTM vs. SVR model for Sylhet and Comilla.

that proves how closely the correlation coefficients (r) are related to the predicted and observed I_F. The hybrid CNN-BiLSTM model in four selected stations with a pool of synoptic climate indices produces a substantially similar output to the observed value than any other applied models. When it came to achieving the closest possible match to the observed data, the proposed model (i.e., CNN-BiLSTM) for the Rangpur and Sylhet stations is the closest. Regardless of improved performance, Ambagan and Chittagong stations showed much deviation from the observed I_F.

The promoting percentage of root means squared error (RMSE), Mean Absolute Error (MAE), and Mean Absolute Percentage Deviation (MAPD) are additional metrics used to evaluate the proposed deep hybrid CNN-BiLSTM model's predictive performance. It should be noted that the BiLSTM and SVR models are compared using the promoting percentage given as the incremental performance (∇) of the objective model over rival techniques. In addition, as shown in Fig. 12, the assessment of ∇_{MAE}, ∇_{MAPD}, and ∇_{RMSE} significantly improves the corresponding parameters as compared to the traditional BiLSTM and SVR models. In the case of ∇_{MAE}, the improvement is 1.1 to 25 % and 0 to 50 % for BiLSTM and SVR accordingly. Similarly, ∇_{MAPD}(%) and ∇_{RMSE}(%) displayed comparable performance ranging from 0 to 89 %, 0 to 98 %, 6.3 to 91.8 %, and 0.2 to 101.3 % for BiLSTM and SVR. This demonstrates that our proposed model was the most responsive forecasting.

4.2. Discussions

Several studies, including Maplecroft (2011) and the United Nations (2015), have identified Bangladesh to be highly susceptible to climate change. Geographically, it is particularly prone to the physical consequences of climate change, with these consequences exacerbating the already-existing sustainability challenges that this densely populated country is dealing with (Mahmud and Prowse, 2012). The harmful effects can be lessened by locating, creating, and validating innovative scientific methodologies that can be used for flood-risk warning and regular monitoring, as well as flood risk reduction and adaptation. In addition, operational flood monitoring and decision-making demand the creation of an index that monitors daily or weekly flood extents, allowing for a more precise assessment of short-term events. A daily flood monitoring index can be used to determine the beginning, length, and intensity of flood event(s) for shorter periods like weeks or months, or longer periods like years (Nosrati et al., 2010).Thus, predicted flood episodes between July 2019 and February 2020 were recorded and quantified for study sites selected based on the diverse classification of I_F as shown in Table 4. In the case of moderate to extreme flood events, it has been observed that the flood began almost the same week, with the longest duration found for the Hatiya station (200 days). Following the application of the CNN-BiLSTM model to a flood situation, it has been discovered that higher flood scenarios provide perfect forecasting with bias error ranges ranging from 0.67 % to 49 %. Chuadanga station performed exceptionally poorly in forecasting results, with a high percentage of bias in the forecasting results (50 %). At the same time, flood warnings were issued for Ambagan, Chittagong, Kepurpara, and Hatiya, which lasted for more than 190 days (consecutive days when I_F>0).

We have addressed essential aspects of flood events, such as flood dangers, flood severity, peak floods, flood duration, and total precipitation. We find that the flood severity and peak flood are precisely the same. Observations have shown that when the flood intensity is highest, the peak flood also appears to be at its highest point. The findings also showed that the I_F was useful for estimating the duration, seriousness, and intensity of flood scenarios as well as for classifying the seriousness

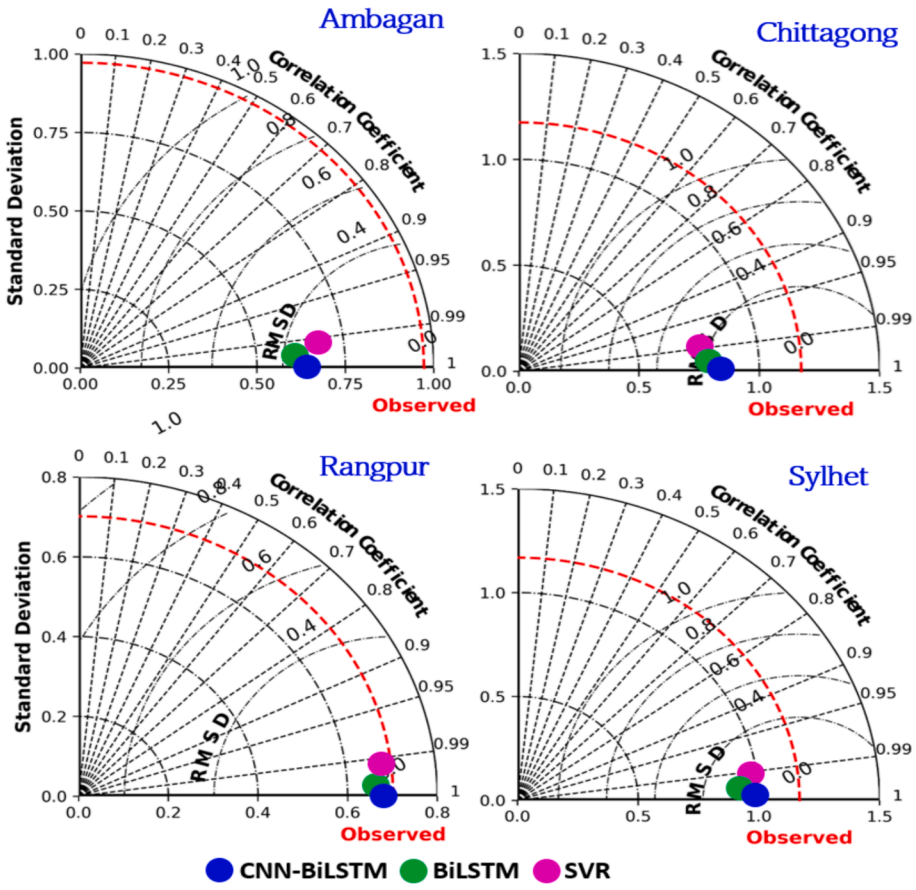

Fig. 11. Tylor diagram representing correlation coefficient and the standard deviation difference for proposed hybrid CNN-BiLSTM vs. benchmark models (i.e., BiLSTM and SVR) for Ambagan, Chittagong, Rangpur, and Sylhet.

of flood situations. It has resulted that the newly developed hybrid CNN-BiLSTM model is based on the flood index feature, which is an important concept to understand. Predicting floods is critical for better flood management and mitigation planning.

The proposed hybrid DL model has been demonstrated to produce a greater prediction of the flood index compared to the standalone models. However, it is important to know that the model's performance is slightly different. It is suggested that the potential serial correlation issue in both the target variable and predictors, indicated by a gradual decrease in the cross-correlations (see Fig. 5), which may lead to problematic issues in significance tests, should be taken into consideration for similar works in the future.

While CNN models show promise in capturing spatial features time series tasks, such as automated speech recognition (Abdel-Hamid et al., 2014) and wind speed forecasting (Wang and Li, 2023), they faces challenges in fully realising temporal features, especially in long-tailed time series associated with a high degree of uncertainty (Afrasiabi et al., 2019). The reason is that CNN models are primarily designed for processing grid-structured data, such as images, where the spatial relationships between neighbouring elements are critical (LeCun et al., 2015). Thus, they are not inherently designed to handle sequential data with temporal dependencies or serial correlation, which is common in time series data. Similarly, SVR models focus on identifying a hyperplane that best fits high-dimensional data (Zhang and O'Donnell, 2020). Although they can capture complex relationships, they do not explicitly consider the temporal dependencies or serial correlation often present in time series data. In addition, while the NCA technique is often used for dimensionality reduction or feature selection tasks, it is not specifically tailored to capture temporal dependencies or address the serial correlation problem in time series data.

To address the serial correlation problem, one solution involves combining CNNs with models explicitly designed to capture dependencies over time, such as recurrent neural networks (RNNs) or other sequence-based models, such as LSTMs or GRUs, as demonstrated in the study by Afrasiabi et al. (2020). The present study addressed the serial correlation problem by combining CNN with BiLSTM in a hybrid model to tackle spatial and temporal aspects simultaneously. BiLSTM models, an extension of traditional LSTMs, process the input sequence in both forward and backward directions (see Section 2.2). This bidirectional processing captures dependencies in both past and future contexts, making it more effective in handling long-term dependencies, and addressing the serial correlation problem. This hybrid approach is applicable and can be particularly effective in other tasks such as video analysis, medical image processing, or time series prediction, where both spatial and temporal aspects play crucial roles. The innovative approach of this study to incorporating climate indices for the real-time prediction of week-ahead flood indexes represents a significant advancement in flood forecasting methodologies. However, the connection between these slowly evolving climate indices, which are typically used to understand long-term climatic variations, and the ability to predict short-term flood events raises intriguing questions about the mechanisms driving this predictive success. To bridge this gap, a detailed exploration into how these indices can influence short-term flood predictions through their impact on local weather patterns and hydrological conditions is essential.

Climate indices, such as the Greenland Block Index (GBI), El Niño Southern Oscillation (ENSO), and Indian Ocean Dipole (IOD), offer insights into the global atmospheric circulation patterns that, in turn, influence regional weather conditions. For instance, the GBI can affect the path and intensity of the westerly winds and storm tracks across the

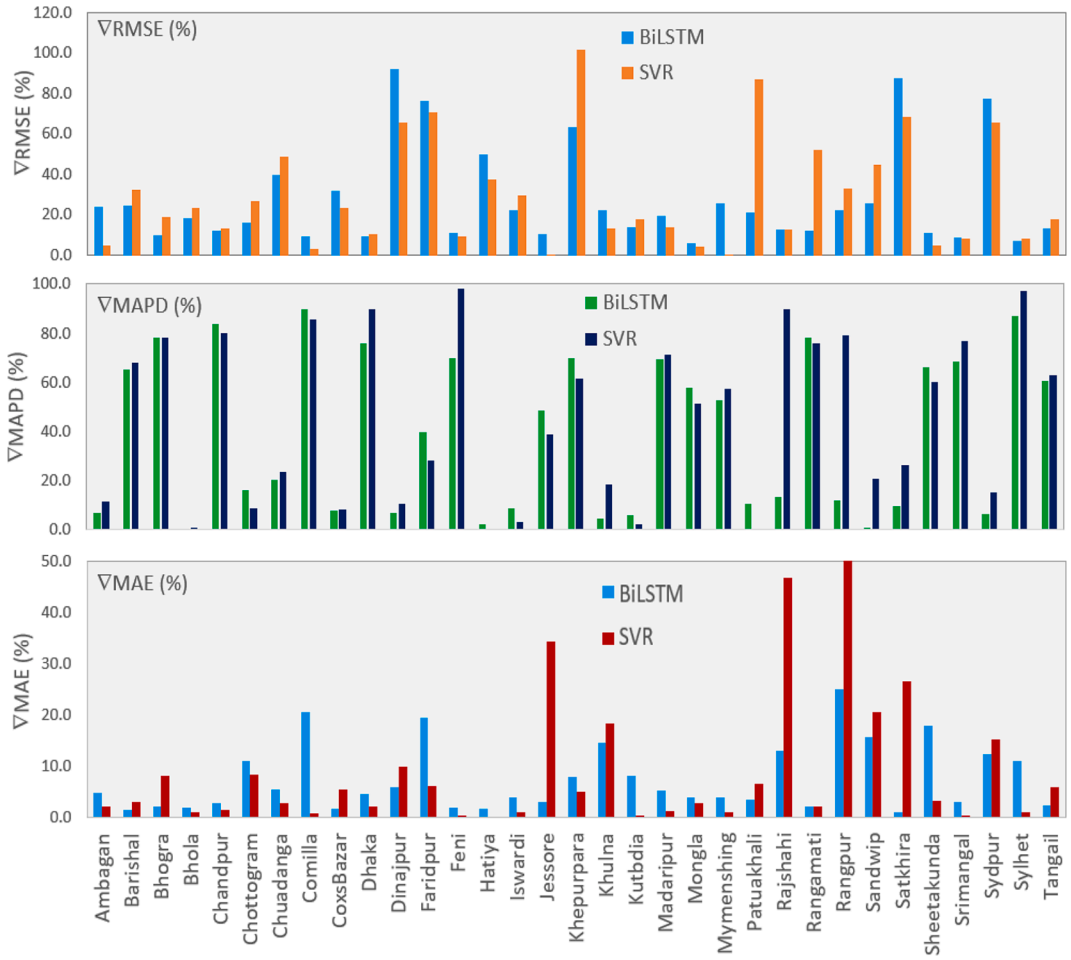

Fig. 12. Promoting Percentage of RMSE ($\nabla RMSE, \%$), MAPD ($\nabla MAPD, \%$), and MAE ($\nabla MAE, \%$) to illustrate the improvement percentage of the proposed model (i.e., CNN-BiLSTM) over standalone models (i.e., BiLSTM and SVR) in I_F forecasting.

Northern Hemisphere, potentially altering precipitation patterns in South Asia, including Bangladesh. The observed higher correlation between the Greenland Block Index (GBI) and the Flood Index (FI) suggests a significant link between atmospheric patterns over Greenland and flood occurrences in the studied region. The GBI is a climate index that quantifies the atmospheric pressure patterns over Greenland, with higher values indicating stronger blocking events. These blocking events can have a profound impact on weather patterns across the Northern Hemisphere, leading to alterations in the jet stream and affecting the distribution of precipitation. When the GBI is in a high phase, it typically results in a redirection of the jet stream, which can lead to prolonged periods of rainfall or dry conditions in different parts of the world, depending on the specific atmospheric setup. In the context of flood prediction, a higher GBI could lead to stagnation of weather systems, increasing the likelihood of prolonged rainfall events downstream, which, in turn, can contribute to higher flood risks.

ENSO, with its phases of El Niño and La Niña, significantly influences the monsoon systems, where El Niño is often associated with reduced monsoon rainfall in South Asia, and La Niña can enhance it, impacting the flood risk in the region. Similarly, positive phases of the IOD are linked to increased rainfall in the Indian subcontinent, which could exacerbate flooding during the monsoon season.

Moreover, exploring existing studies that have investigated the impacts of these climate indices on regional hydrology and weather patterns can provide a solid foundation for understanding their relevance in flood forecasting. For example, research by Ummenhofer et al. (2009) on the impact of IOD on Southeast Asian precipitation and studies by Marengo et al. (2008) on the influence of ENSO on South American hydrology can offer insights into the physical mechanisms through which these indices affect weather patterns conducive to flooding. By delving into the physical relevance of these climate patterns during flood events and their representation in the predictive model, the study could significantly enrich its narrative. This approach would not only validate the inclusion of climate indices in short-term flood forecasting but also provide a comprehensive understanding of the intricate relationships between global climate mode indices and local flood risks.

5. Conclusions and outlook

Deep learning algorithms were used in this paper to develop a new artificial intelligence methodology for daily flood index forecasting. They were trained on synoptic mode indices and reliable ground-truth observations from thirty-four stations in Bangladesh. Our novel method, the hybrid CNN-BiLSTM model combines Convolutional Neural Networks (CNN) with a Bi-directional long short-term Memory (BiLSTM) network. It has been demonstrated that the CNN-BiLSTM model can produce significant improvements in predictive performance and outperform all benchmark models like BiLSTM and SVR.

Upon thorough assessment of the suggested hybrid CNN-BiLSTM model, we have concluded that our method represents a promising approach for developing a predictive model for understanding flood scenarios in Bangladesh. The proposed hybrid CNN-BiLSTM model's superior performance is supported by its high NSE (0.986–0.997) and low MAPD (1.01–3.59) values.

Beyond these prediction issues, the suggested deep hybrid model can be applied to a variety of complicated or difficult prediction tasks,

Table 4
Comparison of Flood Forecasting using the CNN-BiLSTM model between July 2019 and February 2020 and flood severity and duration.

Stations	Onset of Flood	PBIAS (%)	Total Precipitation (mm)	Duration of Flood (Days)
Ambagan	7/7/2019	3.623	6280.96	200
Barisal	10/7/2019	5.605	2204.02	99
Bhola	8/7/2019	5.402	3402.56	185
Bogra	9/25/2019	21.826	298.93	26
Chandpur	N/A			
Chittagong	7/7/2019	21.459	6280.96	199
Chuadanga	10/25/2019	51.897	164.02	6
Comilla	9/7/2019	22.102	2590.98	153
Cox's Bazar	7/7/2019	12.073	5726.64	165
Dhaka	7/8/2019	26.584	887.91	70
Dinajpur	9/23/2019	15.634	437.31	24
Feni	8/8/2019	20.103	1314.44	71
Foridpur	N/A			
Hatiya	7/7/2019	5.699	6477.93	200
Ishwardi	7/8/2019	22.576	1018.06	106
Jessore	08/15/2019	34.561	255.77	11
Khepurpara	5/7/2019	18.652	5570.49	195
Khulna	7/8/2019	13.911	1755.18	130
Kutubdia	5/7/2019	4.701	8106.34	198
Madaripur	7/26/2019	10.345	1634.49	126
Mongla	8/7/2019	6.98	3164.5	190
Mymensingh	9/7/2019	15.768	1955.67	124
Potuakhali	7/7/2019	6.858	4386.58	194
Rajshahi	9/26/2019	25.932	229.66	16
Rangamati	8/7/2019	6.381	3424.57	147
Rangpur	9/14/2019	2.993	561.71	34
Saidpur	09/23/2019	24.231	437.31	23
Swandip	8/13/2019	26.198	423.14	11
Satkhira	8/14/2019	14.971	1407.14	111
Shitakunda	7/7/2019	6.422	6477.93	193
Sreemangal	7/8/2019	8.28	2039.94	143
Sylhet	11/7/2019	17.585	1479.5	48
Tangail	10/7/2019	11.504	1577.38	135
Teknaf	6/30/2019	7.259	6149.95	143

including, among other things, the forecasting of wind speed, energy costs, and tidal energy. Moreover, incorporating global climate models (GCM) to predict the flood index under global warming scenarios for better flood hazard management and mitigation.

CRediT authorship contribution statement

A.A. Masrur Ahmed: Conceptualization, Methodology, Software, Validation, Formal analysis, Investigation, Writing - original draft, Writing - review & editing, Visualization. **Shahida Akther:** Data curation, Formal analysis, Methodology, Writing – review & editing. **Thong Nguyen-Huy:** Methodology, Writing – review & editing. **Nawin Raj:** Writing – review & editing. **S. Janifer Jabin Jui:** Writing – review & editing. **S.Z. Farzana:** Writing – review & editing.

Declaration of competing interest

The authors declare that they have no known competing financial interests or personal relationships that could have appeared to influence the work reported in this paper.

Acknowledgements

The climate mode indices are acquired from different data sources such as the Bureau of Meteorology, Australia, and NCEP. The rainfall data was obtained fron the Bangladesh Meteorological Department, Bangladesh. The flood index was calculated using the Matlab code prescribed by Moishin et al. (2021b). The authors thank all the reviewers and the editor for their thoughtful suggestions and the review process.

References

Abadi, M., Barham, P., Chen, J., Chen, Z., Davis, A., Dean, J., Devin, M., Ghemawat, S., Irving, G., Isard, M., 2016. Tensorflow: A system for large-scale machine learning, 12th {USENIX} Symposium on Operating Systems Design and Implementation ({OSDI} 16), pp. 265-283.

Abdel-Hamid, O., Mohamed, A.-R., Jiang, H., Deng, L., Penn, G., Yu, D., 2014. Convolutional neural networks for speech recognition. IEEE/ACM Trans. Audio Speech Lang. Process. 22, 1533–1545.

Afrasiabi, M., Mohammadi, M., Rastegar, M., Kargarian, A., 2019. Multi-agent microgrid energy management based on deep learning forecaster. Energy 186, 115873.

Afrasiabi, M., Mohammadi, M., Rastegar, M., Afrasiabi, S., 2020. Advanced deep learning approach for probabilistic wind speed forecasting. IEEE Trans. Ind. Inf. 17, 720–727.

Ahmed, A., Deo, R.C., Feng, Q., Ghahramani, A., Raj, N., Yin, Z., Yang, L., 2021a. Hybrid deep learning method for a week-ahead evapotranspiration forecasting. Stoch. Env. Res. Risk A. 1–19.

Ahmed, A., Deo, R.C., Raj, N., Ghahramani, A., Feng, Q., Yin, Z., Yang, L., 2021b. Deep Learning Forecasts of Soil Moisture: Convolutional Neural Network and Gated Recurrent Unit Models Coupled with Satellite-Derived MODIS, Observations and Synoptic-Scale Climate Index Data. Remote Sens. (Basel) 13, 554.

Ahmed, A.A.M., Deo, R.C., Ghahramani, A., Feng, Q., Raj, N., Yin, Z., Yang, L., 2022. New double decomposition deep learning methods for river water level forecasting. Sci Total Environ 831, 154722.

Ahmed, R., Kim, I.-K., 2003. Patterns of daily rainfall in Bangladesh during the summer monsoon season: case studies at three stations. Phys. Geogr. 24, 295–318.

Alam, A., Ahmed, B., Sammonds, P., 2021. Flash flood susceptibility assessment using the parameters of drainage basin morphometry in SE Bangladesh. Quat. Int. 575, 295–307.

Barrett, P., Hunter, J., Miller, J.T., Hsu, J.-C., Greenfield, P., 2005. matplotlib–A Portable Python Plotting Package, Astronomical data analysis software and systems XIV, p. 91.

Bhagabati, S.S., Kawasaki, A., 2017. Consideration of the rainfall-runoff-inundation (RRI) model for flood mapping in a deltaic area of Myanmar. Hydrological Research Letters 11, 155–160.

Bowden, G.J., Dandy, G.C., Maier, H.R., 2005. Input determination for neural network models in water resources applications. Part 1—background and methodology. J. Hydrol. 301, 75–92.

Brammer, H. (1990). Floods in Bangladesh: II. Flood mitigation and environmental aspects. Geographical Journal, 158-165.

BWDB (2019). Summary Of Rainfall In Bangladesh For The Year 2017 & 2018. Surface Water Processing Branch Bangladesh Water Development Board.

Byun, H.-R., Lee, D.-K., 2002. Defining three rainy seasons and the hydrological summer monsoon in Korea using available water resources index. Journal of the Meteorological Society of Japan. Ser. II 80, 33–44.

Cannizzaro, D., Aliberti, A., Bottaccioli, L., Macii, E., Acquaviva, A., Patti, E., 2021. Solar radiation forecasting based on convolutional neural network and ensemble learning. Expert Syst. Appl. 181, 115167.

Chowdhury, M.R., 2005. Consensus seasonal Flood Forecasts and Warning Response System (FFWRS): An alternate for nonstructural flood management in Bangladesh. Environ. Manag. 35, 716–725.

Chowdhury, J. (1998). Some hydraulic aspects of floods in Bangladesh and their implications in planning. Ali, MA, Hoque, MM, Rahman, R., and Rashid, S, 209-217.

Cian, F., Marconcini, M., Ceccato, P., 2018. Normalized Difference Flood Index for rapid flood mapping: Taking advantage of EO big data. Remote Sens. Environ. 209, 712–730.

Deo, R.C., Adamowski, J.F., Begum, K., Salcedo-Sanz, S., Kim, D.-W., Dayal, K.S., Byun, H.-R., 2018. Quantifying flood events in Bangladesh with a daily-step flood monitoring index based on the concept of daily effective precipitation. Theor. Appl. Climatol. 137, 1201–1215.

Ghimire, S., Nguyen-Huy, T., AL-Musaylh, M.S., Deo, R.C., Casillas-Pérez, D., Salcedo-Sanz, S., 2023a. Integrated Multi-Head Self-Attention Transformer model for electricity demand prediction incorporating local climate variables. Energy and AI 14, 100302.

Ghimire, S., Nguyen-Huy, T., AL-Musaylh, M.S., Deo, R.C., Casillas-Pérez, D., Salcedo-Sanz, S., 2023b. A novel approach based on integration of convolutional neural networks and echo state network for daily electricity demand prediction. Energy 275, 127430.

Ghimire, S., Nguyen-Huy, T., Deo, R.C., Casillas-Perez, D., Salcedo-Sanz, S., 2022. Efficient daily solar radiation prediction with deep learning 4-phase convolutional neural network, dual stage stacked regression and support vector machine CNN-REGST hybrid model. Sustain. Mater. Technol. 32, e00429.

Ghimire, S., Nguyen-Huy, T., Prasad, R., Deo, R.C., Casillas-Perez, D., Salcedo-Sanz, S., Bhandari, B., 2023c. Hybrid convolutional neural network-multilayer perceptron model for solar radiation prediction. Cogn. Comput. 15, 645–671.

Ghose, B., Islam, A.R.M.T., Kamruzzaman, M., Moniruzzaman, M., Hu, Z., 2021. Climate-induced rice yield anomalies linked to large-scale atmospheric circulation in Bangladesh using multi-statistical modeling. Theor. Appl. Climatol. 144, 1077–1099.

Gill, E.C., Rajagopalan, B., Molnar, P., 2015. Subseasonal variations in spatial signatures of ENSO on the Indian summer monsoon from 1901 to 2009. J. Geophys. Res. Atmos. 120, 8165–8185.
Hamidi, O., Poorolajal, J., Sadeghifar, M., Abbasi, H., Maryanaji, Z., Faridi, H.R., Tapak, L., 2015. A comparative study of support vector machines and artificial neural networks for predicting precipitation in Iran. Theor. Appl. Climatol. 119, 723–731.
Han, S.U., Byun, H.R., 2006. The existence and the climatological characteristics of the spring rainy period in Korea. Int. J. Climatol. 26, 637–654.
Han, W., Webster, P.J., 2002. Forcing mechanisms of sea level interannual variability in the Bay of Bengal. J. Phys. Oceanogr. 32, 216–239.
Hasnat, G.T., Kabir, M.A., Hossain, M.A., 2018. Major environmental issues and problems of South Asia, particularly Bangladesh. Handbook of Environmental Materials Management 1–40.
Islam, A.R.M.T., Islam, H.T., Shahid, S., Khatun, M.K., Ali, M.M., Rahman, M.S., Ibrahim, S.M., Almoajel, A.M., 2021. Spatiotemporal nexus between vegetation change and extreme climatic indices and their possible causes of change. J. Environ. Manage. 289, 112505.
Kang, H., Yang, S., Huang, J., Oh, J., 2020. Time series prediction of wastewater flow rate by bidirectional LSTM deep learning. Int. J. Control Autom. Syst. 18, 3023–3030.
Ketkar, N., 2017. Introduction to keras. Deep Learning with Python. Springer 97–111.
Khairul, I.M., Rasmy, M., Ohara, M., Takeuchi, K., 2022. Developing Flood Vulnerability Functions through Questionnaire Survey for Flood Risk Assessments in the Meghna Basin. Bangladesh. Water 14, 369.
Kumar, K.K., Rajagopalan, B., Cane, M.A., 1999. On the weakening relationship between the Indian monsoon and ENSO. Science 284, 2156–2159.
LeCun, Y., Boser, B., Denker, J.S., Henderson, D., Howard, R.E., Hubbard, W., Jackel, L. D., 1989. Backpropagation applied to handwritten zip code recognition. Neural Comput. 1, 541–551.
LeCun, Y., Bengio, Y., Hinton, G., 2015. Deep Learning. Nature 521, 436–444.
Li, F., Ma, G., Chen, S., Huang, W., 2021. An Ensemble Modeling Approach to Forecast Daily Reservoir Inflow Using Bidirectional Long-and Short-Term Memory (Bi-LSTM), Variational Mode Decomposition (VMD), and Energy Entropy Method. Water Resour. Manag. 35, 2941–2963.
Lu, E., 2009. Determining the start, duration, and strength of flood and drought with daily precipitation: Rationale. Geophys. Res. Lett. 36.
Mahmud, T., Prowse, M., 2012. Corruption in cyclone preparedness and relief efforts in coastal Bangladesh: Lessons for climate adaptation? Glob. Environ. Chang. 22, 933–943.
Maier, H.R., Jain, A., Dandy, G.C., Sudheer, K.P., 2010. Methods used for the development of neural networks for the prediction of water resource variables in river systems: Current status and future directions. Environ. Model. Softw. 25, 891–909.
Maplecroft, V., 2011. Climate change vulnerability index. Climate change risk atlas 2011. Verisk Maplecroft, United Kingdom.
Masrur Ahmed, A.A., Deo, R.C., Feng, Q., Ghahramani, A., Raj, N., Yin, Z., Yang, L., 2021. Deep learning hybrid model with Boruta-Random forest optimiser algorithm for streamflow forecasting with climate mode indices, rainfall, and periodicity. J. Hydrol. 599.
Matheswaran, K., Alahacoon, N., Pandey, R., Amarnath, G., 2018. Flood risk assessment in South Asia to prioritize flood index insurance applications in Bihar. Geomatics, Natural Hazards and Risk, India.
Moishin, M., Deo, R.C., Prasad, R., Raj, N., Abdulla, S., 2021a. Designing deep-based learning flood forecast model with ConvLSTM hybrid algorithm. IEEE Access 9, 50982–50993.
Moishin, M., Deo, R.C., Prasad, R., Raj, N., Abdulla, S., 2021b. Development of Flood Monitoring Index for daily flood risk evaluation: case studies in Fiji. Stoch. Env. Res. Risk A. 35, 1387–1402.
Nguyen-Huy, T., 2020. Copula-based statistical modelling of synoptic-scale climate indices for quantifying and managing agricultural risks in Australia. Bull. Aust. Math. Soc. 101, 166–169.
Nguyen-Huy, T., Kath, J., Nagler, T., Khaung, Y., Aung, T.S.S., Mushtaq, S., Marcussen, T., Stone, R., 2022. A satellite-based Standardized Antecedent Precipitation Index (SAPI) for mapping extreme rainfall risk in Myanmar. Society and Environment, Remote Sensing Applications, p. 100733.
Nosrati, K., Saravi, M.M., Shahbazi, A., 2010. Investigation of flood event possibility over Iran using Flood Index. Survival and Sustainability. Springer 1355–1361.
Peng, T., Zhang, C., Zhou, J., Nazir, M.S., 2021. An integrated framework of Bi-directional Long-Short Term Memory (BiLSTM) based on sine cosine algorithm for hourly solar radiation forecasting. Energy 221, 119887.
Pothapakula, P.K., Primo, C., Sørland, S., Ahrens, B., 2020. The synergistic impact of ENSO and IOD on Indian summer monsoon rainfall in observations and climate simulations–an information theory perspective. Earth Syst. Dyn. 11, 903–923.
Prasad, R., Deo, R.C., Li, Y., Maraseni, T., 2018. Ensemble committee-based data intelligent approach for generating soil moisture forecasts with multivariate hydro-meteorological predictors. Soil Tillage Res. 181, 63–81.
Prasad, R., Charan, D., Joseph, L., Nguyen-Huy, T., Deo, R.C., Singh, S., 2021a. Daily flood forecasts with intelligent data analytic models: multivariate empirical mode decomposition-based modeling methods, Intelligent Data Analytics for Decision-Support Systems in Hazard Mitigation. Springer 359–381.
Prasad, S.M.M., Nguyen-Huy, T., Deo, R., 2021b. Support vector machine model for multistep wind speed forecasting, Predictive Modelling for Energy Management and Power Systems Engineering. Elsevier 335–389.
Quintero, F., Krajewski, W.F., Rojas, M., 2020. A flood potential index for effective communication of streamflow forecasts at ungauged communities. J. Hydrometeorol. 21, 807–814.
Rahman, M.H., 2010. Ultra Poor Households' Flood Coping Strategies towards Food Security in Two Flood Prone Regions. USAID, Dhaka.
Roy, I., Tedeschi, R.G., 2016. Influence of enso on regional indian summer monsoon precipitation—local atmospheric influences or remote influence from pacific. Atmos. 7, 25.
Taylor, K.E., 2001. Summarizing multiple aspects of model performance in a single diagram. J. Geophys. Res. Atmos. 106, 7183–7192.
Teng, J., Jakeman, A.J., Vaze, J., Croke, B.F., Dutta, D., Kim, S., 2017. Flood inundation modelling: A review of methods, recent advances and uncertainty analysis. Environ. Model. Softw. 90, 201–216.
Tingsanchali, T., Karim, M.F., 2005. Flood hazard and risk analysis in the southwest region of Bangladesh. Hydrological Processes: an International Journal 19, 2055–2069.
Tiwari, M.K., Adamowski, J., 2013. Urban water demand forecasting and uncertainty assessment using ensemble wavelet-bootstrap-neural network models. Water Resour. Res. 49, 6486–6507.
Tiwari, M.K., Chatterjee, C., 2011. A new wavelet–bootstrap–ANN hybrid model for daily discharge forecasting. J. Hydroinf. 13, 500–519.
United-Nations, 2015. International Stratety for Disaster Reduction. Secretariat Global Assessment Report on Disaster Risk Reduction 2015: Making Development Sustainable: the Future of Disaster Risk Management. UN.
Wang, J., Li, Z., 2023. Wind speed interval prediction based on multidimensional time series of Convolutional Neural Networks. Eng. Appl. Artif. Intel. 121, 105987.
Wang, S., Wang, X., Wang, S., Wang, D., 2019. Bi-directional long short-term memory method based on attention mechanism and rolling update for short-term load forecasting. Int. J. Electr. Power Energy Syst. 109, 470–479.
Waskom, M., Botvinnik, O., Ostblom, J., Gelbart, M., Lukauskas, S., Hobson, P., Gemperline, D.C., Augspurger, T., Halchenko, Y., Cole, J.B. (2020). mwaskom/seaborn: v0. 10.1 (April 2020). zenodo.
Xavier, P.K., Marzin, C., Goswami, B.N., 2007. An objective definition of the Indian summer monsoon season and a new perspective on the ENSO–monsoon relationship. Quarterly Journal of the Royal Meteorological Society: A Journal of the Atmospheric Sciences, Applied Meteorology and Physical Oceanography 133, 749–764.
Yang, W., Wang, K., Zuo, W., 2012. Neighborhood Component Feature Selection for High-Dimensional Data. JCP 7, 161–168.
Yevjevich, V.M., 1967. Objective approach to definitions and investigations of continental hydrologic droughts. An. Colorado State University, Libraries.
Zang, H., Liu, L., Sun, L., Cheng, L., Wei, Z., Sun, G., 2020. Short-term global horizontal irradiance forecasting based on a hybrid CNN-LSTM model with spatiotemporal correlations. Renew. Energy 160, 26–41.
Zhang, F., O'Donnell, L.J., 2020. Support vector regression. Machine Learning. Elsevier 123–140.